Ocean Systems Engineering, *Vol. 16, No. 1 (2026) 83-113*
https://doi.org/10.12989/ose.2026.16.1.083

Techno-Press

Stress concentration factors for internally ring stiffened multi-planar tubular DKT-joints of offshore structures

Hamid Ahmadi*[1], Haleh Dasti[2]

[1]*National Centre for Maritime Engineering and Hydrodynamics, Australian Maritime College (AMC), University of Tasmania, Launceston, TAS 7248, Australia*
[2]*Faculty of Civil Engineering, University of Tabriz, Iran*

(Received December 19, 2025, Revised March 5, 2026, Accepted March 9, 2026)

Abstract. Two-planar tubular DKT-joints are widely used in offshore jacket structures, where accurate assessment of stress concentration factors (SCFs) is vital for evaluating fatigue performance. However, SCFs in DKT-joints with internal ring stiffeners have not been thoroughly studied, and no specific design equations currently exist for determining SCFs under axial loading which is typically the dominant load in these joints. In practice, engineers often rely on SCF data from uniplanar KT-joints to estimate values for multi-planar joints. This approach, however, overlooks the influence of out-of-plane braces, potentially resulting in significant inaccuracies. This study addresses this gap by analyzing SCFs on the chord side of ring-stiffened two-planar tubular DKT-joints under axial brace loading. The investigation is based on 118 finite element (FE) models, validated through both experimental data and existing numerical results. A comprehensive parametric FE study was conducted, followed by nonlinear regression analyses to derive four new equations that accurately predict SCFs. These proposed formulas offer a reliable tool for fatigue design applications.

Keywords: fatigue; internal ring stiffener; offshore jacket structure; stress concentration factor (SCF); two-planar tubular DKT-joint

1. Introduction

Jacket structures are commonly used in offshore industry as the substructure of fixed offshore oil and gas platforms and offshore wind turbines (OWTs). They are steel space frames composed of welded circular hollows section (CHS) members also called tubulars. The connection between the tubulars in which the prepared ends of brace members are welded onto the undisturbed surface of the chord member is called a tubular joint (Fig. 1). Static and fatigue strengths of tubular joints are governing factors in the design of jacket structures.

Tubular joints must be properly dimensioned during the design stage so that they perform satisfactorily in service and achieve a reasonable balance between the project cost and risk of failure. If the capacity of a joint is found to be inadequate during the design stage, it can be enhanced by welding ring stiffeners onto the inner surface of the chord (Fig. 1) as this is an efficient method to reduce the stress concentration, increase the load-carrying capacity and fatigue

*Corresponding author, Ph.D., E-mail: hamid.ahmadi@utas.edu.au

http://www.techno-press.org/ose/5
ISSN: 2093-6702 (Print), 2093-677X (Online)

life of the joint, and avoid the attraction of additional wave forces. None of the major offshore design codes provides any substantial quantitative recommendations on fatigue strength requirements for internally ring-stiffened joints. This is due partly to the vast variety of possible stiffening arrangements and partly to the dearth of information available on such joints in research literature. There is, therefore, a need for further research so that more detailed guidelines on fatigue strength estimation of internally ring-stiffened tubular joints can be formulated, which is the incentive of the present work.

Significant stress concentrations at the vicinity of the welds are considerably detrimental to the fatigue performance of the joints. Hence, it is important to accurately determine the magnitude of stress concentration and to reduce it to a reasonable level. In the design practice, a parameter called the stress concentration factor (SCF) is used to evaluate the magnitude of stress concentration. The SCF is defined as the ratio of the local surface stress at the brace-chord intersection to the nominal stress in the brace. More specifically, the local surface stress used for the calculation of the SCF, as defined by API RP 2A [1], is the linear trend of shell bending and membrane stress, extrapolated to the actual weld toe, excluding the local notch effects of weld shape. The local surface stress calculated in this manner is called the hot-spot stress (HSS).

The value of the SCF exhibits considerable scatter depending on the joint geometry, loading type, weld size and type, and the considered position for the SCF calculation along the weld profile. Under any specific loading condition, the SCF value along the weld toe of a tubular joint is mainly determined by joint geometry. To study the behavior of tubular joints and to easily relate this behavior to the geometrical characteristics of the joint, a set of dimensionless geometrical parameters has been defined. Fig. 1 depicts an internally ring-stiffened two-planar tubular DKT-joint with the geometrical parameters τ, γ, β, η, ζ, θ, α, and α_B; where D and d are the diameters of the chord and brace, respectively; L and l are the lengths of those members, respectively; and T, t, and w_s are the chord thickness, brace thickness, and stiffener width, respectively. Critical positions along the weld toe of the brace-chord intersection for the calculation of SCFs in a tubular joint, i.e., saddle, crown, toe, and heel on the chord side of central and outer braces are shown in Fig. 1.

Significant effort has been devoted to the study of SCFs in various uniplanar tubular joints (i.e., joints where the axes of the chord and brace members lay on the same plane). As a result, many parametric design formulas in terms of the joint's geometric parameters have been proposed providing SCF values at certain positions adjacent to the weld for several loading conditions. An extensive survey of the literature is provided in the following section. Multi-planar joints (i.e., joints where the axes of the chord and all brace members do not lay on the same plane) are an intrinsic feature of offshore tubular structures. The multi-planarity effect might play an important role in the stress distribution along the brace-to-chord intersection. Thus, for multi-planar connections, the parametric formulas of simple uniplanar tubular joints may not be applicable for the SCF prediction since such formulas may lead to highly over-/under-predicting results. Nevertheless, for multi-planar joints which cover most practical applications, much fewer investigations have been reported due to the complexity and high cost involved.

In the present paper, results of a numerical investigation on the SCFs in two-planar tubular DKT-joints reinforced with internal ring stiffeners are presented and discussed. In this research program, a set of parametric finite element (FE) stress analyses was carried out on 118 internally ring-stiffened tubular DKT-joint models subjected to axial loading (Fig. 1). Analysis results were used to present general remarks on the effects of geometrical parameters including τ (brace-to-chord thickness ratio), γ (chord wall slenderness ratio), β (brace-to-chord diameter ratio), θ (brace inclination angle), and η (ring width to chord diameter ratio) on the SCFs at crown, toe, and saddle

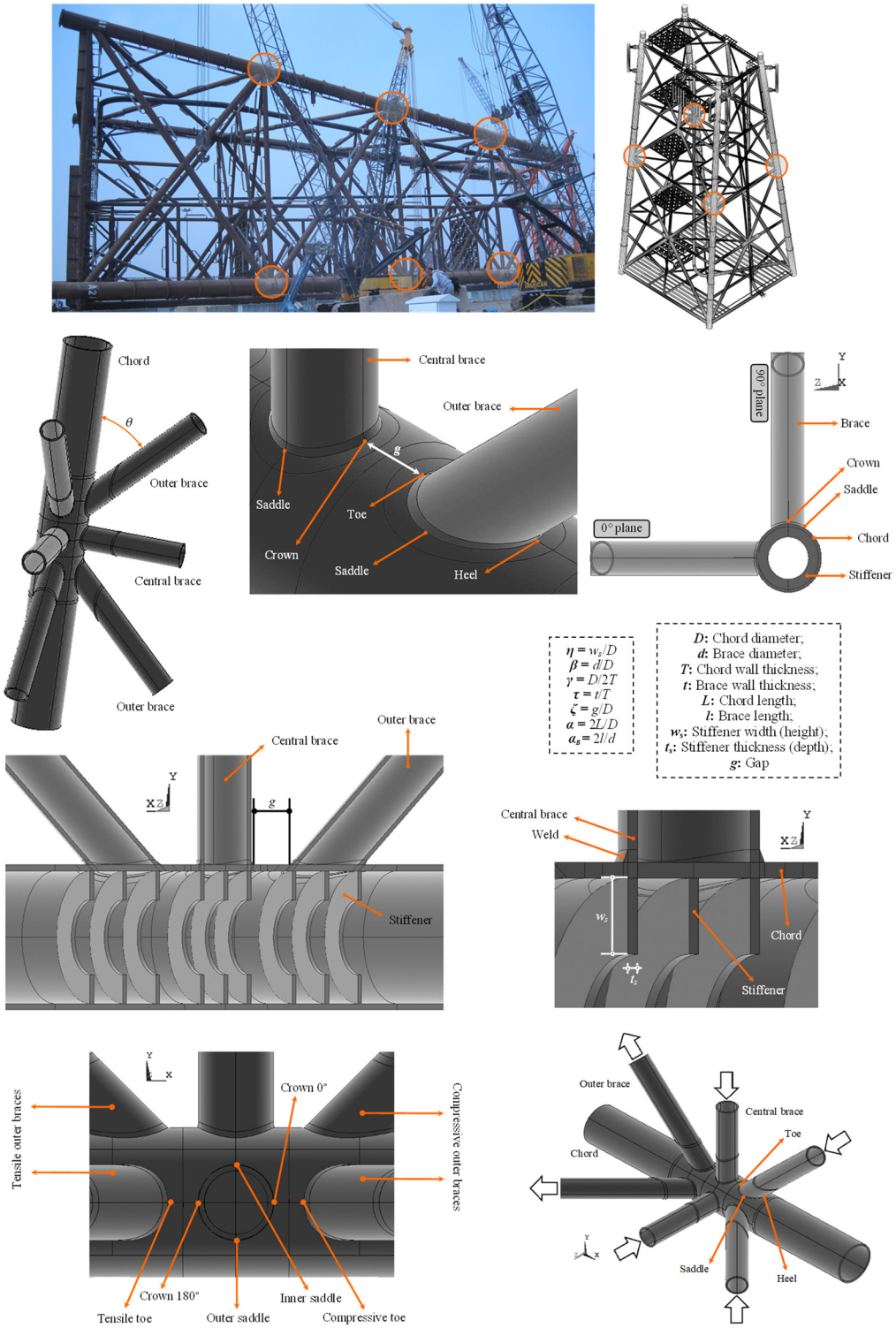

Figure 1. Two-planar DKT-joints in jacket structures, geometrical notations, and studied axial loading

positions on the chord side of central and outer braces. Based on the results of internally ring-stiffened DKT-joint FE models, verified against experimental and numerical data, an SCF database was prepared. Afterwards, a new set of SCF parametric equations was established, based on nonlinear regression analyses, for the fatigue design of two-planar tubular DKT-joints reinforced with internal ring stiffeners subjected to axial loading. The reliability of proposed equations was evaluated according to the acceptance criteria recommended by the UK Department of Energy [2].

2. Literature survey

2.1 SCFs in unreinforced tubular joints

2.1.1 SCFs in unreinforced uniplanar connections

For the study of SCFs in various uniplanar tubular joints, the reader is referred to [3], [4], [5], [6], [7] for the SCF calculation at the saddle and crown positions of simple uniplanar T-, Y-, X-, K-, and KT-joints; and [8], [9], [10], [11] for the SCF determination in overlapped uniplanar joints, among others. For the study of SCF distribution along the weld toe in uniplanar tubular joints, the reader is referred for example to [12, 13] for K-joints; [14, 15] for T-, Y-, X-, and DT-joints; [16, 17], [18] for T- and K-joints; [19], [20], [21] for KT- and DKT-joints; and [22] for T-joints.

2.1.2 SCFs in unreinforced multi-planar connections

For the SCF studies in multi-planar joints, the reader is referred to [23] and [24] for the SCF calculation in XX-joints; [25] for the SCF determination in KK-joints; [26] for the study of SCFs in DT-joints; [27] for the study of SCFs in XT-joints; [28, 29], [30], and [31] for the investigation of SCFs in multi-planar KT-joints under axial loads; [32] for the SCF determination in unreinforced XT-joints subjected to out-of-plane bending (OPB) moment loadings; and [33] for the analysis of SCFs in two-planar tubular joints of OWTs, among others.

2.2 SCFs in reinforced tubular joints

2.2.1 SCFs in reinforced uniplanar connections

For the SCF calculation at saddle and crown positions of stiffened tubular joints, the reader is referred for example to [34] for ring-stiffened T-joints; [35] for doubler-plate reinforced T-joints; [36] for rack-plate reinforced joints; [37] and Ahmadi and Zavvar [38] for ring-stiffened KT-joints subjected to in-plane bending (IPB) moment and OPB moment loadings; [39] for concrete-filled joints.

Ahmadi et al. [40, 41] investigated the SCF distribution along the weld toe of central and outer braces in tubular KT-joints reinforced with internal ring stiffeners and proposed a set of parametric equations to calculate the SCFs along the brace-to-chord intersection in internally ring-stiffened KT-joints subjected to axial loading. Nassiraei and Rezadoost [42-45] investigated the stress concentration in tubular T/Y- and X-joints retrofitted with fiber-reinforced polymer (FRP) composites subjected to axial and bending loads. Nassiraei and Rezadoost [46, 47] studied the SCFs in tubular T-joints stiffened with external rings subjected to axial and bending loads. Zavvar and Guedes Soares [48] investigated the SCFs in FRP strengthened uniplanar DKT-joints.

2.2.2 SCFs in reinforced multi-planar connections

Woghiren and Brennan [49] developed a set of parametric equations to predict the SCFs at critical positions along the brace-to-chord intersection in two-planar tubular KK-joints reinforced with rack plates. Ahmadi et al. [50] conducted a comprehensive stress concentration analysis on internally ring-stiffened tubular KK-joints.

2.3 Other SCF-related studies in various tubular joints

For other SCF-related investigations such as probabilistic and reliability studies, the reader is referred for example to [51], [52], [53], [54], [55], [56], [57], [58], [59], [60].

2.4 Study of ultimate strength, degree of bending (DoB), and local joint flexibility (LJF)

Azari-Dodaran et al. [61, 62] and Azari-Dodaran and Ahmadi [63] studied the ultimate strength of axially loaded K- and KT-joints at fire-induced elevated temperatures. Nassiraei [64-68] investigated the ultimate strength of tubular T/Y- and X-joints reinforced with collar plates at ambient and elevated temperatures based on deterministic and probabilistic approaches.

Zavvar et al. [69] published a comprehensive review on the analysis of tubular joints in marine structures. Ahmadi and Asoodeh [70] investigated the DoB in tubular K-joints subjected to OPB loadings. Nassiraei et al. [71] and Nassiraei [72] studied the DoB values for X-joints retrofitted with FRP composites.

Ahmadi and Ziaei Nejad [73] investigated the LJF in two-planar DK-joints of OWTs subjected to axial loading. Nassiraei [74-77] studied the LJF in T/Y- and X-joints stiffened with collar and doubler plates. Ahmadi and Akhtegan [78] and Ahmadi and Akbari Niri [79] investigated the LJF in three-planar T- and Y-joints in offshore structures.

2.5 Remarks

It can be clearly concluded from Sects. 2.1-2.4 that, over the past five decades, significant effort has been devoted to the study of SCF, ultimate strength, DoB, and LJF in various unstiffened tubular joints including both uniplanar and multi-planar connections. Albeit the majority of these studies are on uniplanar joints. However, the study of SCFs in stiffened joints is rather limited. It is also evident that in the case of stiffened joints, almost all available research reports are on the SCFs in uniplanar connections and the studies on the SCFs in multi-planar stiffened joints are quite rare. Despite the application of two-planar tubular DKT-joints reinforced with internal ring stiffeners in the design of offshore jacket-type structures, the SCFs in internally ring-stiffened DKT-joints have not been investigated and no design equation is currently available to determine the weld-toe SCFs in this type of joint.

3. FE modeling

3.1 Internal ring stiffeners

The simplest and most accurate way to model the interaction between the chord and the stiffener is to glue their volumes during the geometrical modeling by which the generated mesh for

these volumes will be automatically merged. However, this straight-forward method is not applicable in the present study. The reason is that gluing the volumes of the chord and the stiffener during the geometrical modeling will produce serious problems in generating a high-quality mesh around the brace-to-chord intersection. Consequently, due to the poor quality and irregularity of the generated mesh along the brace-to-chord intersection, it is almost impossible to accurately determine the extrapolated stresses (HSSs) along the intersection based on the stresses perpendicular to the weld toe. In such a situation, only the SCF at the saddle position may be extracted accurately. In the present study, to resolve this issue, the chord and stiffener were meshed separately and then the ANSYS contact capability was used to define the interaction between them. In problems involving contact between two boundaries, one of the boundaries is conventionally established as the "target" surface and the other as the "contact" surface. In this study, the outer surfaces of the rings were introduced as the target surface and inner surface of the chord was established as the contact surface. Flexible-to-flexible surface-to-surface contact elements were used to simulate the interaction. The augmented Lagrange method was used as the contact algorithm and the behavior of the contact surface was defined to be always bonded. Contact was set to be detected on Gauss points and be automatically adjusted to close the gap and reduce the penetration.

For axial loading, the most effective position for ring stiffeners has been found to be the middle half of the plug [34]. However, the use of a single stiffener at the saddle position is not recommended since it produces a region of high local stiffness through which a high proportion of the load is transferred causing high SCFs on the chord and brace side [36]. Hence, as shown in Fig. 1, three ring stiffeners were used for each brace member in all models: One at the saddle position and the other two at the crown positions. To avoid high stress concentrations in the stiffener, thickness of the stiffener (t_s) should not be less than the brace wall thickness (t). On the other hand, according to [34], the inertia moment of the stiffener, in the radial direction of the chord, is the main factor in controlling the SCFs. This result suggests that using thin tall stiffeners can lead to optimum SCF values. Hence, the stiffener thickness was designated to be equal to the brace wall thickness in all models of the present study.

3.2 Weld profile

Accurate modeling of the weld profile is one of the most critical factors affecting the accuracy of SCF results. Therefore, the weld sizes must be carefully included in the FE modeling. Several research works has been carried out on the study of the weld effect. For example, the reader is referred to [80], [81], [82], among others. It was found that the fatigue strength of the joint can be underestimated by 20% compared to the experimental data when the weld is not considered [83].

In the present study, the welding size along the brace-to-chord intersection satisfies the AWS D 1.1 [84] specifications. According to these specifications, the weld sizes at the crown, saddle, toe, and heel positions can be determined as follows

$$H_w(\text{mm}) = 0.85t(\text{mm}) + 4.24$$
$$L_w = \frac{t}{2}\left[\frac{135^\circ - \psi\ (\text{deg.})}{45^\circ}\right] \tag{1}$$

$$\psi = \begin{cases} 90^\circ & \text{Crown} \\ 180^\circ - \cos^{-1}\beta \text{ (deg.)} & \text{Saddle} \\ 180^\circ - \theta \text{ (deg.)} & \text{Toe} \\ \theta \text{ (deg.)} & \text{Heel} \end{cases},$$

The parameters used in Eq. (1) are defined in Fig. 2. The dihedral angle (ψ) which is an important parameter in determining the weld thickness is defined as the angle between the chord and brace surface along the intersection curve. Details of the weld profile modeling according to [84] have been presented by Ahmadi et al. [85].

It should be noted that attempts to produce an improved as-welded profile often result in over-welding. Consequently, the actual weld size, typical of yard practice, is usually different from the nominal weld size recommended by AWS D 1.1 [84]. For the correction of SCFs to consider the actual position of the weld toe, the reader is advised to follow the recommendations of Sect. B.8.3.2 of API RP 2A [1].

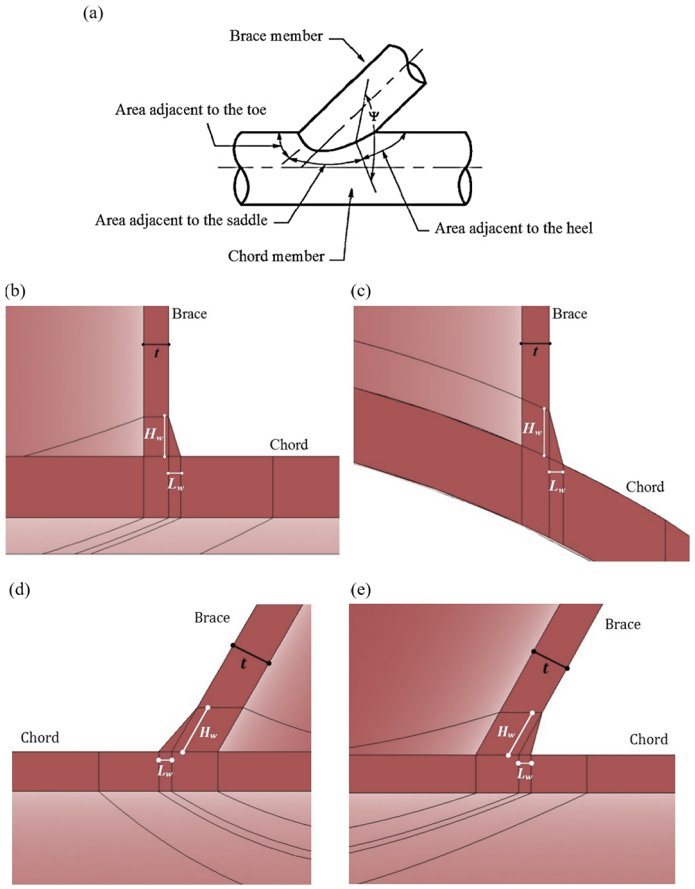

Figure 2 (a) Definition of the dihedral angle, (b) Weld dimensions at the saddle position, (c) Weld dimensions at the crown position, (d) Weld dimensions at the toe position and (e) Weld dimensions at the heel position

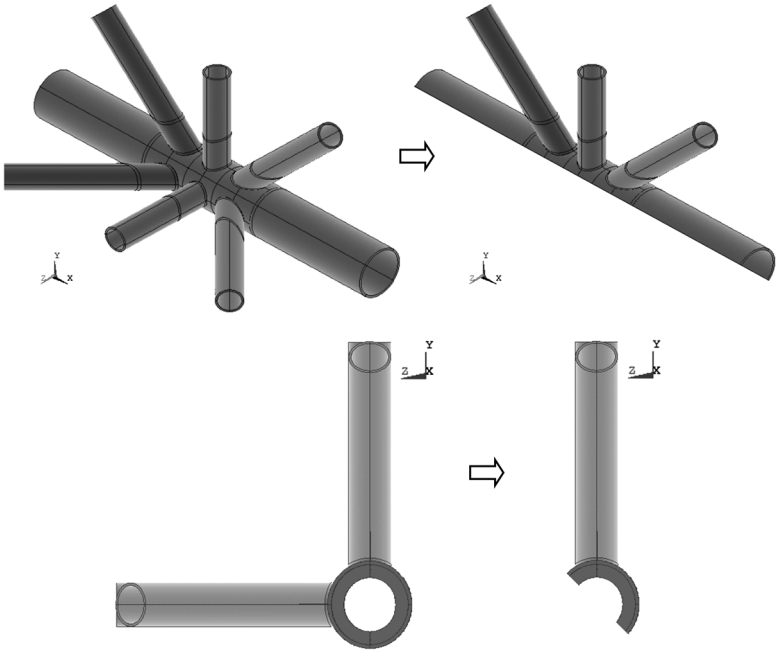

Figure 3. Half of the entire two-planar tubular DKT-joint required to be modeled under studied axial loading condition

Considering the effect of possible weld defects, it should be noted that for fatigue design purposes, the hot-spot stress (HSS) method has been quite efficient and popular in which the local weld effects such as the sharp notch, undercut and crack-like defects at the weld toe are included in the *S-N* curve. According to this method, the nominal stress at the joint members is multiplied by an appropriate SCF to provide the HSS at a certain location. HSSs are calculated at various positions around the weld and the maximum HSS range (S) is determined. Then, the fatigue life of the joint is estimated through an appropriate *S-N* fatigue curve, N being the number of load cycles. The HSS range concept places different structural geometries on a common basis, enabling them to be treated using a single *S-N* curve. The basis of this concept is to capture stress (or strain) in the proximity of the weld toes, which characterizes the fatigue life of the joint, but excludes the stress increase due to the local notch of the weld toe. As stated before, the local weld notch effects are included in the *S-N* curve.

3.3 Boundary conditions

In offshore structures, the chord end fixity conditions of tubular joints may range from almost fixed to almost pinned with generally being closer to almost fixed [4]. In practice, the value of the parameter α in over 60% of tubular joints is in excess of 20 and is bigger than 40 in 35% of the joints [86]. Changing the end restraint from fixed to pinned results in a maximum increase of 15% in the SCF at the crown position for joints with $\alpha = 6$, and this increase reduces to only 8% for $\alpha = 8$ [13]. In the view of the fact that the effect of chord end restraints is only significant for joints with $\alpha < 8$ and high β and γ values, which do not commonly occur in practice, both chord ends were assumed to be fixed, with the corresponding nodes restrained.

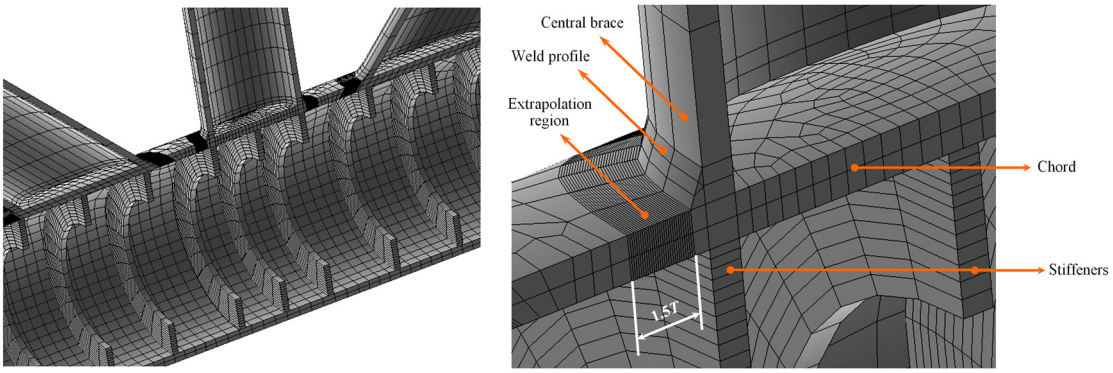

Figure 4. Generated mesh based on the sub-zone scheme

Due to the symmetry in geometry and loading of the joint, only half of the entire internally ring-stiffened tubular DKT-joint is required to be modeled to reduce the computational time (Fig. 3). Appropriate symmetric boundary conditions were defined for the nodes located on the symmetry planes.

3.4 Mesh

Both shell and 3D solid (brick) elements are commonly used for the FE analysis. The choice of element type for the analysis depends on the geometry of the joint and the purpose for which the results of the analysis are to be used. It must be a compromise between accuracy of representation and the computer time taken to analyze a particular model [15]. The 3D brick elements can be used to model the entire tubular joint. Using this type of element, the weld profile can be modeled as a sharp notch. This method will produce more accurate and detailed stress distribution near the intersection in comparison with a simple shell analysis. The most important disadvantage for using shell elements is that this type of element is not suitable to model the weld and consequently some details of the 3D stresses in the joint are lost. This is the main reason why there are some discrepancies between the thin shell FE results and those obtained from experimental tests. However, shell element was used by most researchers in early stages because it is much easier to generate the mesh and it was less expensive in computer time to compute the stresses in the tubular joints. Nowadays, the advances in the technology of computer processors lead to a considerable reduction in the computer time needed to analyze solid models. It is worth mentioning here that for certain applications which require detailed information in the vicinity of the weld and through the wall thickness of the members, such as fracture mechanics studies of small cracks in tubular joints, solid elements are essential.

In the present study, ANSYS element SOLID95 was used to model the chord, braces, rings, and weld profiles. This element type has compatible displacements and is well-suited to model curved boundaries. It is defined by 20 nodes having three degrees of freedom per node and may have any spatial orientation.

To guarantee the mesh quality, a sub-zone mesh generation scheme was used during the FE modeling. The entire structure was divided into several zones according to computational requirements. The mesh of each zone was generated separately and then the mesh of the entire joint was produced by merging the meshes of all the sub-zones. This scheme can feasibly control

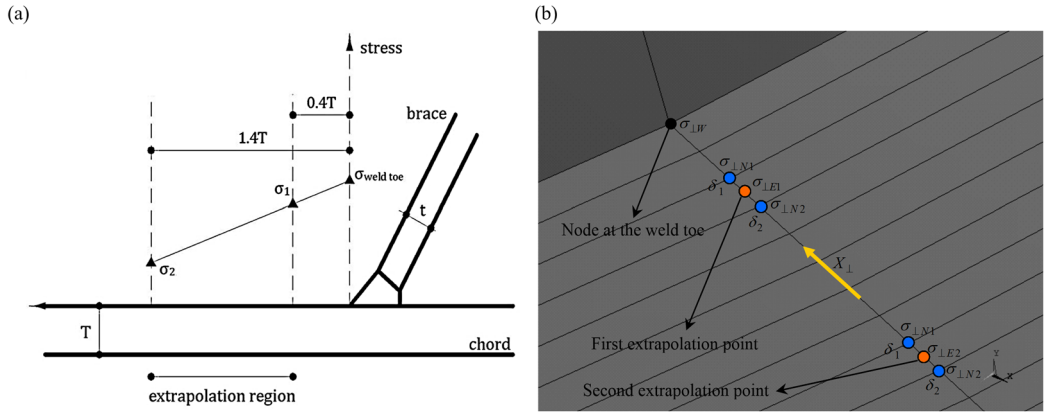

Figure 5. (a) Extrapolation method according to IIW XV-E [88] and (b) Required interpolations and extrapolations to extract the HSS value at the weld toe

the mesh quantity and quality and avoid badly distorted elements. The mesh generated by this procedure for an internally ring-stiffened tubular DKT-joint is shown in Fig. 4.

As mentioned earlier, to determine the SCF, the HSS at the weld toe should be divided by the nominal stress of the loaded brace. The stresses perpendicular to the weld toe at the extrapolation points are required to be calculated to determine the stress at the weld toe position. To extract and extrapolate the stresses perpendicular to the weld toe, as shown in Figs. 4 and Fig. 5(b), the region between the weld toe and the second extrapolation point was meshed finely in such a way that each extrapolation point was placed between two nodes located in its immediate vicinity. These nodes are located on the element-generated paths which are perpendicular to the weld toe.

To verify the convergence of FE results, convergence tests with different mesh densities were conducted before generating the 118 FE models for parametric study.

3.5 Analysis and SCF extraction

Static analysis of the linear elastic type is suitable to determine the SCF in a tubular joint [87]. The Young's modulus and Poisson's ratio were taken to be 207 GPa and 0.3, respectively.

The weld-toe SCF is defined as

$$\text{SCF} = \sigma_{\perp W} / \sigma_n , \tag{2}$$

In Eq. (2), σ_n is the nominal stress of the axially loaded brace; and $\sigma_{\perp W}$ is the extrapolated stress at the weld toe position which is perpendicular to the weld toe. Values of σ_n and $\sigma_{\perp W}$ are calculated by Eqs. (3) and (4), respectively.

$$\sigma_n = \frac{4F_a}{\pi\left[d^2 - (d-2t)^2\right]}, \tag{3}$$

where F_a is the applied axial force; and d and t are brace diameter and thickness, respectively.

To calculate the SCF, the stress at the weld toe position should be extracted from the stress field outside the region influenced by the local weld toe geometry. The location from which the

stresses must be extrapolated, *extrapolation region*, depends on the dimensions of the joint and on the position along the intersection. According to the linear extrapolation method recommended by IIW XV-E [88], the first extrapolation point must be at $0.4T$ from the weld toe, and the second point should lie at $1.0T$ further from the first point (Fig. 5(a)). Hence, based on the extrapolation method recommended by IIW XV-E [88], $\sigma_{\perp W}$ in Eq. (2) should be calculated by the following equation

$$\sigma_{\perp W} = 1.4\sigma_{\perp E1} - 0.4\sigma_{\perp E2}, \tag{4}$$

where $\sigma_{\perp E1}$ and $\sigma_{\perp E2}$ are the stresses at the first and second extrapolation points along the direction perpendicular to the weld toe, respectively.

Stress at an extrapolation point is obtained as follows

$$\sigma_{\perp E} = \frac{\sigma_{\perp N1} - \sigma_{\perp N2}}{\delta_1 - \delta_2}(\Delta - \delta_2) + \sigma_{\perp N2}, \tag{5}$$

where $\sigma_{\perp Ni}$ (i = 1 and 2) is the nodal stress at the immediate vicinity of the extrapolation point along the direction perpendicular to the weld toe (Eq. (6)); δ_i (i = 1 and 2) is the distance between the weld toe and the considered node inside the extrapolation region (Eq. (7)); and Δ equals to $0.4T$ and $1.4T$ for the first and second extrapolation points, respectively (Fig. 5(b)).

$$\sigma_{\perp N} = \sigma_x {l_1}^2 + \sigma_y {m_1}^2 + \sigma_z {n_1}^2 + 2\left(\tau_{xy} l_1 m_1 + \tau_{yz} m_1 n_1 + \tau_{zx} n_1 l_1\right), \tag{6}$$

$$\delta = \sqrt{(x_w - x_n)^2 + (y_w - y_n)^2 + (z_w - z_n)^2}, \tag{7}$$

In Eq. (6), σ_a and τ_{ab} (a, b = x, y, z) are components of the stress tensor which can be extracted from ANSYS analysis results; and l_1, m_1, and n_1 are transformation components defined as

$$l_1 = \cos(X_\perp, x); m_1 = \cos(X_\perp, y); n_1 = cos(X_\perp, z), \tag{8}$$

where $X_\perp$ is the direction perpendicular to the weld toe; and x, y, and z are axes of the global coordinate system (Fig. 5(b)). These components can be calculated as below

$$l_1 = (x_w - x_n)/\delta; m_1 = (y_w - y_n)/\delta; n_1 = (z_w - z_n)/\delta, \tag{9}$$

where (x_n , y_n , z_n) and (x_w , y_w , z_w) are global coordinates of the considered node inside the extrapolation region and its corresponding node at the weld toe position, respectively.

At the saddle, crown, toe, and heel positions, Eq. (6) is simplified as

$$\sigma_{\perp N} = \sigma_y {m_1}^2 + \sigma_z {n_1}^2 + 2\tau_{yz} m_1 n_1 \text{ (Saddle)} ; \sigma_{\perp N} = \sigma_x \text{ (Crown, toe, and heel)} , \tag{10}$$

To facilitate the SCF calculation, the above formulation was implemented in a *macro* developed in the ANSYS Parametric Design Language (APDL). The input data required to be provided by the user of the macro are the node number at the weld toe, the chord thickness, and the numbers of the nodes inside the extrapolation region. These nodes can be introduced using the Graphic user interface (GUI).

Regarding the type of stress to be used for the SCF calculation, it should be noted that in earlier studies, SCF calculations were based mostly on the maximum principal stress. Alternatively, the primary stress defined as the stress normal to the weld toe can be used. According to [7], in crown

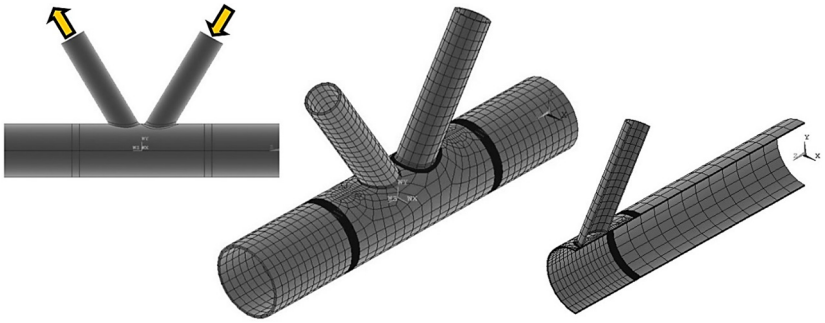

Figure 6. Validating FE model generated for the comparison of results with HSE OTH 354 [6] experimental measurements

positions of K-joints, primary and principal stresses coincide and differences in saddle positions are negligible. As stated before, in the present study, primary stress was employed exclusively.

Regarding the extrapolation method to be used for the HSS determination, it should be noted that Lloyd's Register has reviewed 67 T/Y-, X-, and K-joints that employed both linear and non-linear extrapolation of stresses to the brace-to-chord intersection to calculate the HSS. It was concluded that non-linear extrapolation exceeds linear extrapolation on the chord side for all load cases by less than 5% irrespective of brace angle [6]. As stated before, the linear extrapolation method recommended by IIW XV-E [88] was used in the present study.

3.6 Verification

As far as the authors are aware, there is no experimental/numerical data available in the literature on the SCFs in internally ring-stiffened two-planar tubular DKT-joints that are studied in the present research. However, a set of related experimental and numerical data is available that can be used for the verification of present FE models. The method of geometrical modeling (introducing the chord, brace, stiffener, and weld profile), the mesh generation procedure (including the selection of element type and size), load application, analysis method, and the method of SCF extraction were identical for the validating FE models and the DKT-joint models used for parametric study. Hence, the verification of SCF values derived from validating FE models with the available experimental/numerical data lends some support to the validity of SCF values derived from the DKT-joint models of present paper.

3.6.1 HSE OTH 354 [6] experimental data

Experimental data on the SCFs of uniplanar K-joints published in HSE OTH 354 [6] was used to validate the present FE models. In order to do so, an FE model was generated for a K-joint having the same geometrical characteristics as the K-4 specimen (Table 1) and the model was analyzed subjected to balanced axial loading (Fig. 6). Results of verification process are presented in Table 2 which shows that there is a good agreement between the results of present FE model and experimental data, where the difference between the results is about 7%.

3.6.2 Numerical results of Nwosu et al. [34]

Nwosu et al. [34] presented a set of numerical results for the estimation of SCFs in axially loaded uniplanar tubular T-joints reinforced with internal ring stiffeners (Fig. 7). This data was

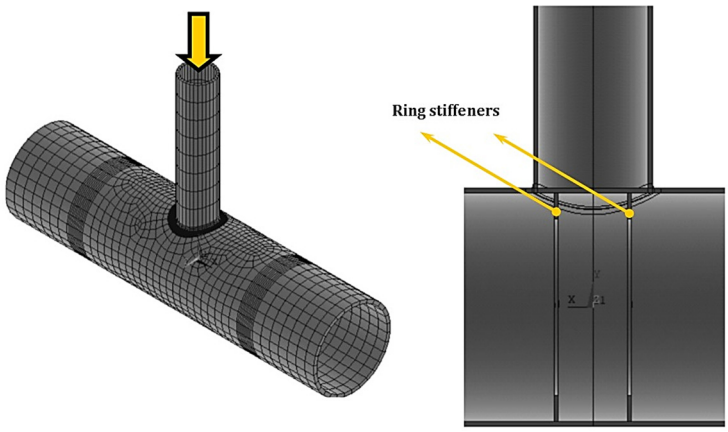

Figure 7. Validating FE model to compare the results with the numerical data from Nwosu et al. [34]

Table 1. Properties of uniplanar tubular K-joint used for the verification of present FE model

Joint ID [6]	Material	Loading type	D (mm)	τ	β	γ	θ	α	ζ
K-4	Steel	Axial	216	0.88	0.47	13.5	60°	10.2	0.11

Table 2. Results of the FE model verification based on HSE OTH 354 [6] experimental data

Position	SCF		Difference
	Present FE model	HSE OTH 354 [6] experimental data	
Toe	5.8	5.4	6.9%

Table 3. Properties of internally ring-stiffened T-joint used for the verification of present FE model

Loading type	D (mm)	d (mm)	T (mm)	t (mm)	L (mm)	l (mm)	w_s (mm)	t_s (mm)	Δ_s* (mm)
Axial	914	457	16	16	2458	1828	100	16	266

*Δ_s: Distance between stiffeners

Table 4. Results of the FE model verification based on experimental and numerical data provided by Nwosu et al. [34]

Position	SCF		Difference
	Present FE model	Nwosu et al. [34] numerical results	
Saddle	8.30	7.30	12.0%
Crown	3.69	4.00	7.7%

used in the present study to validate the generated FE models. To do so, an FE model was generated for an internally ring-stiffened T-joint having the same geometrical characteristics as an FE model generated by Nwosu et al. [34] and the model was analyzed subjected to axial loading (Table 3). Results of verification process are presented in Table 4. There is a good agreement between the results of present FE model and the data provided by Nwosu et al. [34], where the average difference is less than 10%.

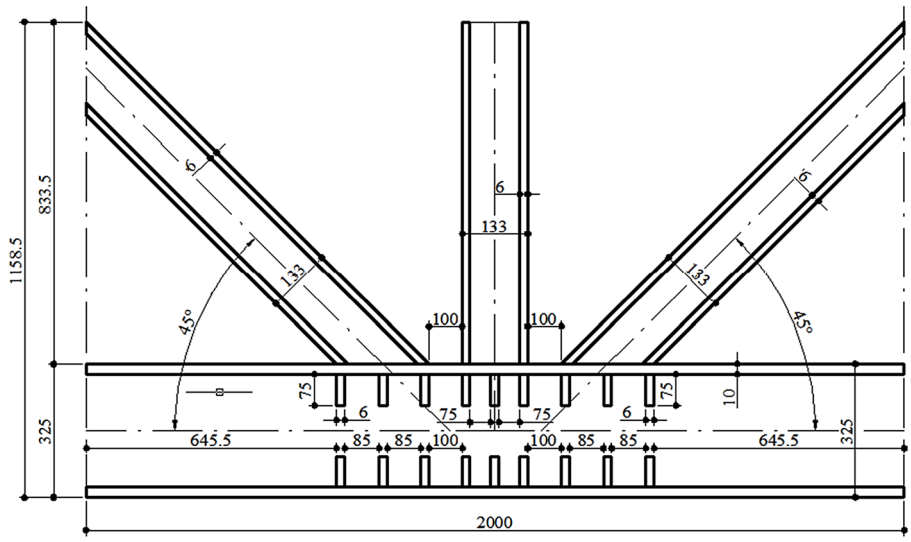

Dimensionless geometrical parameters:
$\tau = 0.60$, $\gamma = 16.25$, $\beta = 0.41$, $\eta = 0.23$, $\zeta = 0.31$, $\alpha = 12.31$

Figure 8. Geometrical properties of the steel uniplanar KT-joint reinforced with internal ring stiffeners used for the validation of developed FE models [40]

3.6.3 Numerical results of Ahmadi et al. [40]

A validating FE model was generated, and its results were compared with the results of numerical modeling carried out by the first author on a uniplanar KT-joint reinforced with internal ring stiffeners (Fig. 8). Results of verification process are presented in Table 5 which shows that there is a good agreement between the results of present FE model and numerical data provided by Ahmadi et al. [40] where the average difference is 5.7%.

3.6.4 Experimental results of Ahmadi [89]

Results obtained from a validating FE model were compared with the results of experimental tests and numerical modeling carried out by the first author on an unstiffened two-planar tubular DKT-joint (Fig. 9). The geometrical properties of the tested specimen were as depicted in Fig. 8 without the stiffeners. Results of verification process are presented in Table 6. It can be seen that there is a good agreement between the results of present FE model and experimental data provided by Ahmadi [89] and the average difference is 5.4%.

Sects. 3.6.1-3.6.4 indicate that generated FE models can be considered to be accurate enough to provide valid and reliable results.

Table 5. Results of the FE model verification based on numerical data provided by Ahmadi et al. [40] on the SCFs in a uniplanar KT-joint reinforced with internal ring stiffeners

Position	SCF		Difference
	Present FE model	Ahmadi et al. [40] numerical results	
Saddle	1.36	1.43	5.1%
Crown	1.35	1.27	6.3%

(a) Test setup for unstiffened two-planar DKT-joint

(b) Arrangement of strain gauges

(c) Data-logging device

Figure 9. Setup of the experimental test on unstiffened two-planar DKT-joint used for the validation of developed FE models [89]

Table 6. Results of the FE model verification based on experimental data provided by Ahmadi [89] on the SCFs in an unstiffened two-planar tubular DKT-joint

Position	SCF		Difference
	Present FE model	Ahmadi [89] experimental data	
Saddle	4.43	4.82	8.8%
Crown	2.97	3.03	2.0%

4. Geometrical effects on the SCFs

4.1 Details of parametric study

In order to study the SCFs in two-planar tubular DKT-joints reinforced with internal ring stiffeners subjected to axial loading (Fig. 1), 118 models were generated and analyzed using the FE software, ANSYS. The objective was to investigate the effects of non-dimensional geometrical parameters on the chord-side SCFs at various positions along the weld toe.

It should be noted that only the brace members were loaded, and no axial loading was applied to the chord member. According to Sect. B.8.3.1 of API RP 2A [1], although nominal cyclic stresses in the chord member also contribute to fatigue loading, their contribution is usually small. The reason is that, unlike brace loading, chord loading does not cause any significant local bending of the chord walls. Hence, any stress raising effects are minimal. The effect of nominal cyclic stresses in the chord member may be covered by including the stress due to axial load in the chord can member, with SCF = 1.25, at the chord crown location only, accounting for sign and phase differences with other brace load effects. Contributions at other locations, namely at the saddle and the brace side are considerably smaller and may be neglected. For the special case of a structure in which the cyclic loads in the chords dominate, the braces can be regarded as non-load carrying attachments and checked with an appropriate *S-N* curve.

Table 7. Values assigned to dimensionless parameters

Parameter	Definition	Value(s)
β	d/D	0.3, 0.4, 0.5
γ	$D/2T$	12, 18, 24
τ	t/T	0.4, 0.7, 1.0
θ	Brace inclination angle	30°, 45°, 60°
η	w_s/D	0.1, 0.15, 0.2
ζ	g/D	0.3
α	$2L/D$	16
α_B	$2l/d$	8

Different values assigned for parameters β, γ, τ, θ, and η are presented in Table 7. These values cover the practical ranges of the dimensionless parameters typically found in tubular joints of offshore jacket structures.

Providing that the gap between the brace members is not very large, the relative gap ($\zeta = g/D$) has no considerable effect on the SCF values. The validity range for this conclusion is $0.2 \leq \zeta \leq 0.6$ [19]. Hence, a typical value of $\zeta = 0.3$ was designated for all joints.

A sufficiently long chord greater than six chord diameters (i.e. $\alpha \geq 12$) must be used to ensure that the stresses at the brace-to-chord intersection are not affected by the end condition [4]. Hence, in this study, a realistic value of $\alpha = 16$ was designated for all the models. The brace length has no effect on SCFs when the parameter α_B is greater than a critical value [14]. This critical value is about 6 [90]. In the present study, to avoid the effect of short brace length, a realistic value of $\alpha_B = 8$ was assigned to all joints.

The 118 generated models span the following ranges of geometric parameters

$$\begin{gathered} 0.3 \leq \beta \leq 0.5 \\ 12 \leq \gamma \leq 24 \\ 0.4 \leq \tau \leq 1.0 \\ 30^{\circ} \leq \theta \leq 60^{\circ} \\ 0.1 \leq \eta \leq 0.2, \end{gathered} \tag{2}$$

4.2 Effects of parameters τ, β, γ, θ, and η on SCF values

Parameter τ is the ratio of brace thickness to chord thickness and γ is the ratio of radius to thickness of the chord. Hence, the increase of the τ in models having constant value of γ results in the increase of the brace thickness. Four charts are given in Fig. 10, as an example, depicting the change of chord-side SCFs at crown 0° and crown 180° positions (Fig. 1) due to the change in the value of τ and the interaction of this parameter with γ. A large number of comparative charts were used to study the effect of τ on the SCFs and only four of them are presented here for the sake of brevity. Results showed that the increase of τ leads to the increase of SCFs at all the considered positions. This result is not dependent on the values of other geometrical parameters.

Parameter β is the ratio of brace diameter to chord diameter. Hence, the increase of β in models having constant value of chord diameter results in the increase of brace diameter. Fig. 11 demonstrates the change of SCFs at compressive toe and tensile toe positions (Fig. 1) due to the

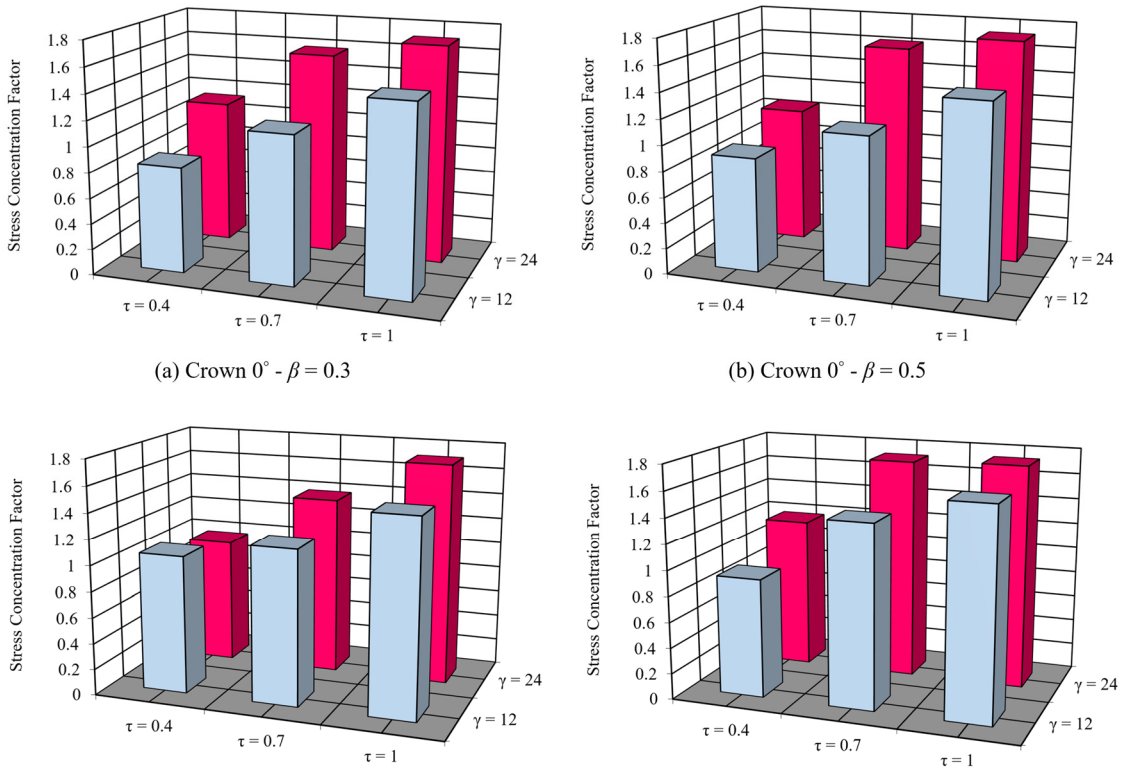

(a) Crown 0° - $\beta = 0.3$

(b) Crown 0° - $\beta = 0.5$

(c) Crown 180° - $\beta = 0.3$

(d) Crown 180° - $\beta = 0.5$

Figure 10. The effect of τ on the SCFs and its interaction with γ ($\theta = 30^{\circ}$, $\eta = 0.15$)

change in the value of β and the interaction of this parameter with θ. Through investigating the effect of β on SCFs, it can be concluded that the increase of β generally leads to the increase of SCFs at the considered positions.

Parameter γ is the ratio of radius to thickness of the chord. Hence, the increase of γ in models having constant value of the chord diameter means the decrease of chord thickness. Four charts are presented in Fig. 12 depicting the change of SCFs at crown 0° and crown 180° positions (Fig. 1) due to the change in the value of γ and the interaction of this parameter with β. It was observed that the increase of γ results in the increase of SCFs at the considered crown, toe, and saddle positions.

The parameter θ is the brace inclination angle. Fig. 13 shows the change of SCF values at compressive toe and tensile toe positions (Fig. 1) due to the change in the value of θ and the interaction of this parameter with γ. Results show that the increase of θ leads to the increase of the SCF. This result is not dependent on the values of other geometrical parameters.

The parameter η is the ratio of the stiffener width to the chord diameter. Hence, the increase of η in models having constant value of the chord diameter means the increase of the stiffener width. Fig. 14 shows the change of the SCF values at crown 0° and crown 180° positions (Fig. 1) due to the change in the value of η and the interaction of this parameter with τ. Results show that the increase of η leads to the decrease of SCFs at all the considered positions.

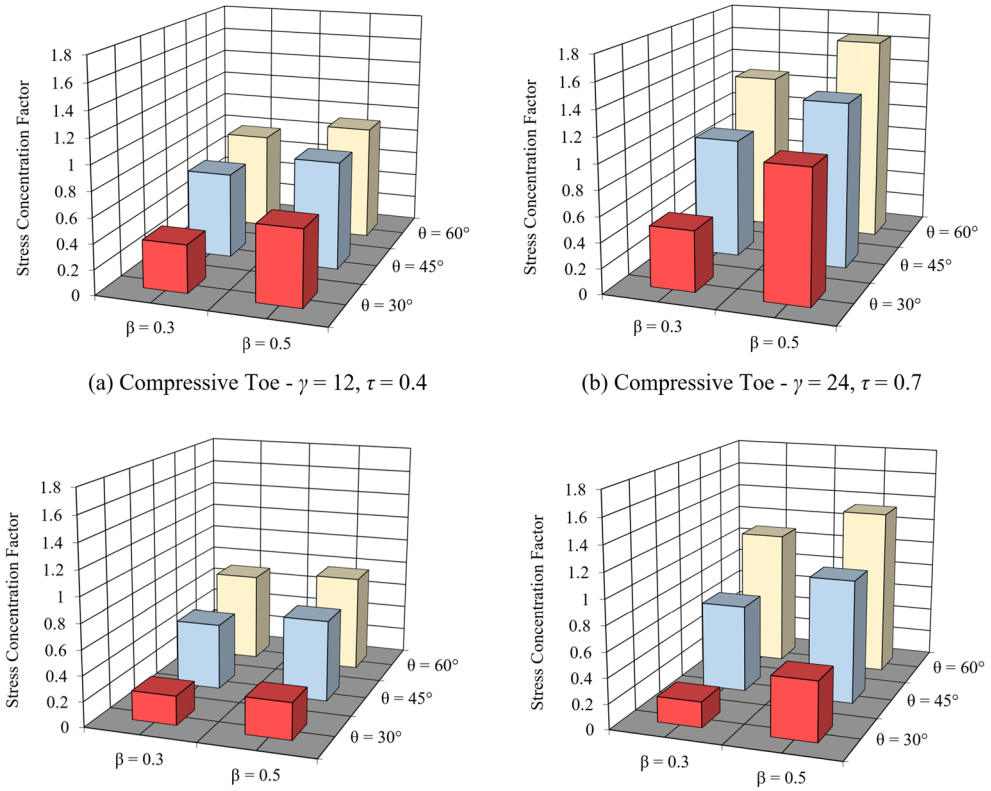

(a) Compressive Toe - $\gamma = 12$, $\tau = 0.4$

(b) Compressive Toe - $\gamma = 24$, $\tau = 0.7$

(c) Tensile Toe - $\gamma = 12$, $\tau = 0.4$

(d) Tensile Toe - $\gamma = 24$, $\tau = 0.7$

Figure 11. The effect of β on the SCFs and its interaction with θ ($\eta = 0.15$)

4.3 Remarks on the biggest and smallest SCF values

By comparing the SCFs at the positions considered, it can be concluded that

$$SCF_{C180} > SCF_{C0} > SCF_{CT} > SCF_{TT} > SCF_{IS} > SCF_{OS}, \quad (12)$$

where SCF_{C180}, SCF_{C0}, SCF_{CT}, SCF_{TT}, SCF_{IS}, and SCF_{OS} denote the SCF values at the crown 180°, crown 0°, compressive toe, tensile toe, inner saddle, and outer saddle positions, respectively (Fig. 1).

It should be noted that a limit on minimum SCF is necessary for conservative design of tubular joints under fatigue loading. A limit of SCF = 1.5 is recommended for simple tubular joints by API RP 2A [1], UEG [91], Smedley and Fisher [86], [15]. Efthymiou and Durkin [92] proposed that the limit of minimum SCF for overlapping joints could be lowered to 1.0 for the chord-side SCFs.

4.4 Remarks on the effects of stiffeners on SCFs

The SCF values in unstiffened and internally ring-stiffened DKT-joints are compared in Fig. 15 indicating that there is a significant difference between the SCF values in two-planar KT-joints with and without internal ring stiffeners. It can be clearly observed that the internal ring stiffeners

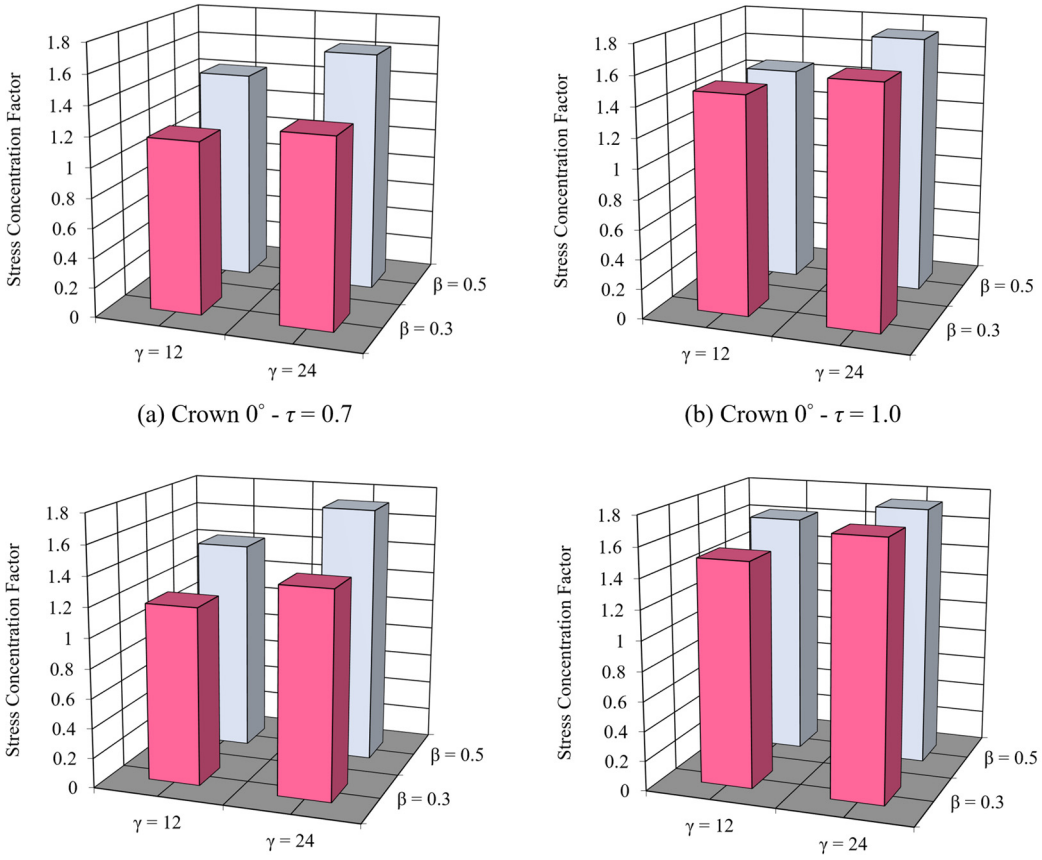

(a) Crown 0° - $\tau = 0.7$ (b) Crown 0° - $\tau = 1.0$

(c) Crown 180° - $\tau = 0.7$ (d) Crown 180° - $\tau = 1.0$

Figure 12. The effect of γ on the SCFs and its interaction with β ($\theta = 30^{\circ}$, $\eta = 0.15$)

can significantly reduce the SCFs in DKT-joints which consequently leads to considerable increase in the fatigue life of tubular joint. For example, the SCF value at the crown 180° position of a sample stiffened joint model ($\eta = 0.1$, $\beta = 0.4$, $\gamma = 24$, $\tau = 0.7$, $\theta = 45^{\circ}$) is 4.8 times the SCF value at the crown 180° position of the corresponding unstiffened joint. Hence, it can be concluded that for axially loaded ring-stiffened DKT-joints, the parametric formulas of unstiffened DKT-joints are not applicable for the SCF prediction, since such formulas lead to highly over-predicting results. Consequently, developing a set of specific parametric equations for the SCF calculation in internally ring-stiffened DKT-joints subjected to axial loading would be beneficial for design purposes.

5. Derivation of design equations to calculate the SCFs

Four individual parametric equations are proposed in the present paper, to calculate the SCFs at the crown 0°, crown 180°, compressive toe, and tensile toe positions on the weld toe of two-planar tubular DKT-joints reinforced with internal ring stiffeners subjected to axial loading (Fig. 1).

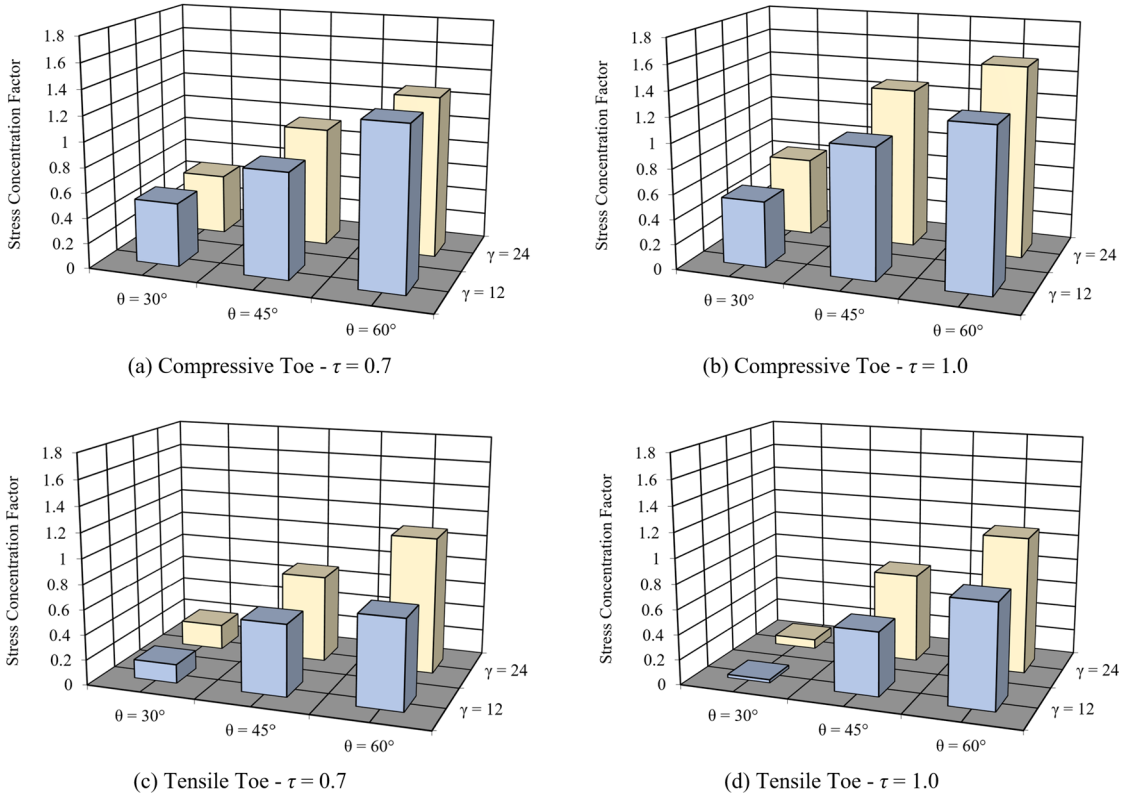

(a) Compressive Toe - $\tau = 0.7$ (b) Compressive Toe - $\tau = 1.0$

(c) Tensile Toe - $\tau = 0.7$ (d) Tensile Toe - $\tau = 1.0$

Figure 13. The effect of θ on the SCFs and its interaction with γ ($\beta = 0.3$, $\eta = 0.15$)

Since the values of SCF at the inner saddle and outer saddle positions are usually less than unity, no parametric equation is required for these positions and a minimum value of 1.0 can be adopted for design purposes.

Results of multiple nonlinear regression analyses performed by SPSS were used to develop these parametric SCF design formulas. Values of dependent variable (i.e., SCF) and independent variables (i.e., β, γ, τ, θ, and η) constitute the input data imported in the form of a matrix. Each row of this matrix involves information about the SCF value at a considered position on the weld toe of an internally ring-stiffened two-planar tubular DKT-joint having specific geometrical properties.

When the dependent and independent variables are defined, a model expression must be built with defined parameters. Parameters of the model expression are unknown coefficients and exponents. The researcher must specify a starting value for each parameter, preferably as close as possible to the expected final solution. Poor starting values can result in failure to converge or in convergence on a solution that is local (rather than global) or is physically impossible. Various model expressions must be built to derive a parametric equation having a high coefficient of determination (R^2).

The following parametric equations are proposed, after performing a large number of nonlinear analyses, for the calculation of chord-side SCFs at the crown 0°, crown 180°, compressive toe, and tensile toe positions in two-planar tubular DKT-joints reinforced with internal ring stiffeners subjected to axial loading (Fig. 1).

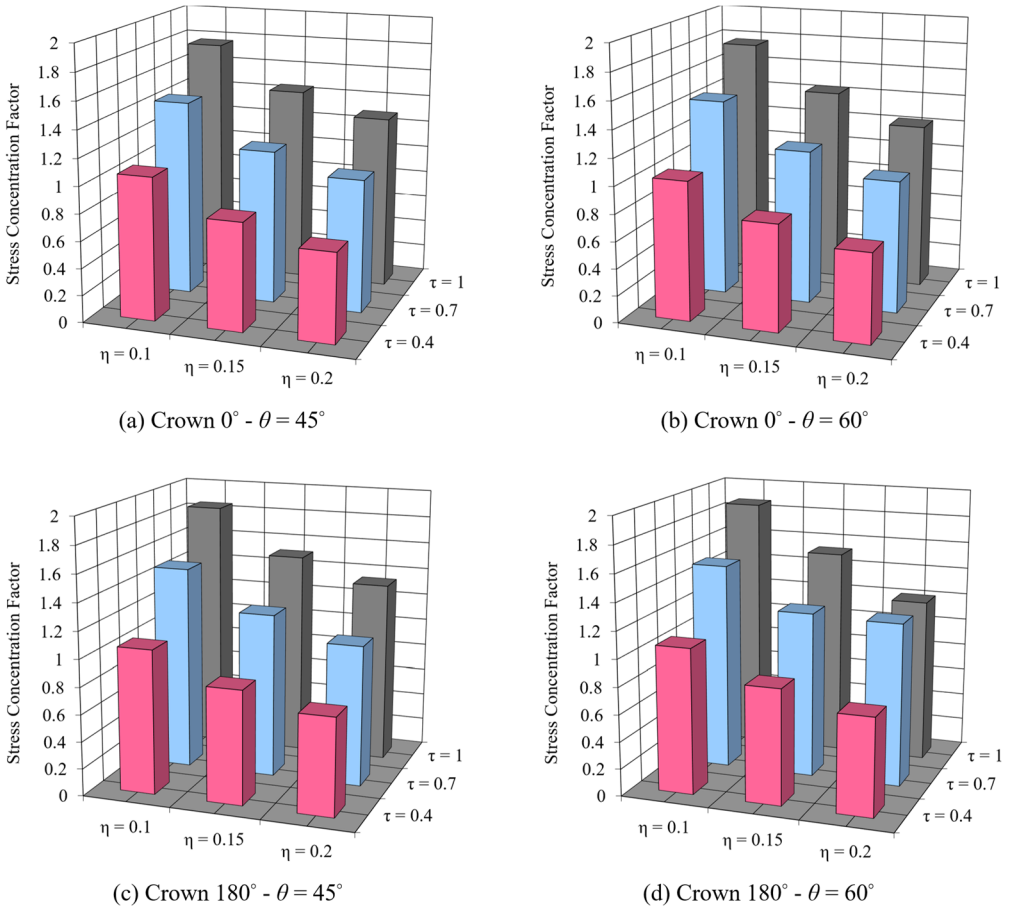

(a) Crown 0° - $\theta = 45°$ (b) Crown 0° - $\theta = 60°$

(c) Crown 180° - $\theta = 45°$ (d) Crown 180° - $\theta = 60°$

Figure 14. The effect of η on the SCFs and its interaction with τ ($\beta = 0.3$, $\gamma = 12$)

Crown 0° position:

$$\mathrm{SCF_{C0}} = 0.685\beta^{0.291}\gamma^{0.166}\tau^{1.038}\eta^{-0.506}\theta^{-0.052} \cdot \cos(0.308\beta + 1.036\gamma - 1.102\tau + 0.407\eta + 0.812\theta) \;\; ; \;\; R^2 = 0.825, \tag{13}$$

Crown 180° position:

$$\mathrm{SCF_{C180}} = 0.746\beta^{0.39}\gamma^{0.741}\sqrt{\tau^{2.784}}\,\eta^{-0.386}\theta^{1.199} \cdot \cos(-0.084\beta + 1.033\gamma - 0.474\tau - 0.232\eta - 0.621\theta) \;\; ; \;\; R^2 = 0.824, \tag{14}$$

Compressive toe position

$$\mathrm{SCF_{CT}} = 0.65\beta^{1.063}\,\gamma^{-0.318}\tau^{0.658}\eta^{-0.587}\theta^{2.275} \cdot (-8.899\beta + 0.199\gamma - 0.823\tau + 0.12\eta - 13.452\theta + 19.705) \;\; ; \;\; R^2 = 0.902, \tag{15}$$

Tensile toe position:

$$\mathrm{SCF_{TT}} = 0.016\beta^{0.175}\gamma^{0.477}\tau^{0.560}\eta^{-0.797}\theta^{-0.722} \cdot (1.507\beta + 0.003\gamma - 1.996\tau - 5.1\eta + 8.353\theta - 2.025) \;\; ; \;\; R^2 = 0.962, \tag{16}$$

Figure 15. Comparison of SCF values in unstiffened and internally ring-stiffened DKT-joints ($\beta = 0.4$, $\gamma = 24$, $\tau = 0.7$, $\theta = 45^{\circ}$, $\eta = 0.1$)

Table 8. Results of equation assessment according to the UK Department of Energy [2] acceptance criteria

Proposed equation	Conditions		Decision
	$\%P/R < 0.8$	$\%P/R > 1.5$	
Eq. (13)	2.5% < 5% OK.	5.9% < 50% OK.	Accept
Eq. (14)	1.7% < 5% OK.	2.5% < 50% OK.	Accept
Eq. (15)	4.2% < 5% OK.	0.8% < 50% OK.	Accept
Eq. (16)	6.8% > 5%	6.8% < 50% OK.	Revise

Dimensionless parameters used in Eqs. (13)-(16) are defined in Fig. 1. SCF_{C0}, SCF_{C180}, SCF_{CT}, and SCF_{TT} denote the SCF values at the crown 0°, crown 180°, compressive toe, and tensile toe positions, respectively, as shown in Fig. 1. Values obtained for R^2 are acceptable considering the complex nature of the problem. The validity ranges of dimensionless geometrical parameters for the developed equations are given in Eq. (11).

In Fig. 16, the SCF values predicted by proposed equations are compared with the SCFs extracted from FE analyses. It can be seen that there is a good agreement between the results of proposed equations and numerically computed values.

The UK Department of Energy [2] recommends the following assessment criteria regarding the applicability of the commonly used SCF parametric equations (P/R stands for the ratio of the *predicted* SCF from a given equation to the *recorded* SCF from test or analysis):

- For a given dataset, if % SCFs under-predicting ≤ 25%, i.e. [$\%P/R < 1.0$] ≤ 25%, and if% SCFs considerably under-predicting ≤ 5%, i.e., [$\%P/R < 0.8$] ≤ 5%, then accept the equation. If, in addition, the percentage SCFs considerably over-predicting ≤ 50%, i.e., [$\%P/R > 1.5$] ≥ 50%, then the equation is regarded as generally conservative.

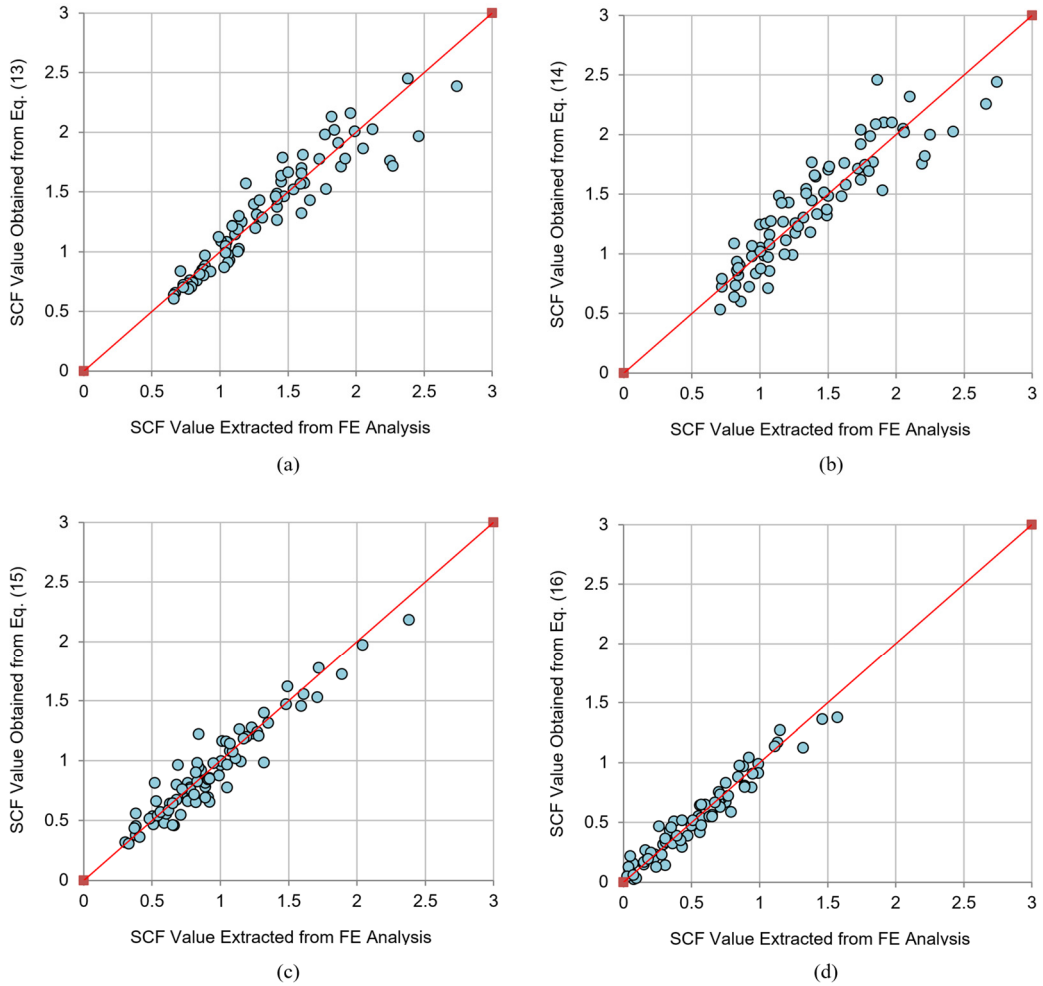

Figure 16. Comparison of 118 SCF values calculated by each of the proposed equations with the corresponding SCFs extracted from the FE analysis: (a) Eq. (13), (b) Eq. (14), (c) Eq. (15) and (d) Eq. (16)

- If the acceptance criteria is nearly met i.e., 25% < [%P/R < 1.0] ≤ 30%, and/or 5% < [%P/R < 0.8] ≤ 7.5%, then the equation is regarded as borderline and engineering judgment must be used to determine acceptance or rejection.
- Otherwise reject the equation as it is too optimistic.

In view of the fact that for a mean fit equation, there is always a large percentage of under-prediction, the requirement for joint under-prediction, i.e., P/R < 1.0, can be completely removed in the assessment of parametric equations [93]. Assessment results according to the UK Department of Energy [2] criteria are presented in Table 8.

For example, we had 118 SCF values at the crown 0° position extracted from the numerical analysis of 118 FE models which means that we had 118 R values at the tensile toe position. We also had 118 SCF values obtained from Eq. (13) based on the dimensionless geometrical parameters of 118 generated FE models meaning that we also had 118 P values. Hence, altogether

we had 118 P/R values at the crown 0° position that only three of them were smaller than 0.8 resulting in [%P/R < 0.8] = 3/118 = 0.0254 = 2.5% which is the number mentioned in the second column of Table 8.

Table 8 shows that Eqs. (13)-(15) satisfy the criteria recommended by the UK Department of Energy, but Eq. (16) requires revision. To revise Eq. (16), the SCF values calculated from this equation were multiplied by a coefficient in such a way that the obtained SCF set satisfies the UK DoE acceptance criteria. This idea can be expressed as follows

$$\text{Design Factor} = \text{SCF}_{\text{Design}} / \text{SCF}_{\text{Eq}}, \tag{17}$$

where the values of $\text{SCF}_{\text{Eq.}}$ are calculated from the proposed equation and the values of $\text{SCF}_{\text{Design}}$ are expected to satisfy the UK DoE criteria.

Multiple comparative analyses were carried out to determine the optimum value of the design factor. Results showed that the optimum design factor for Eq. (16) is 1.07. Hence, the following equations should be used for design purposes.

$$\text{Design Factor} = \text{SCF}_{\text{Design}} / \text{SCF}_{\text{Eq}}, \tag{18}$$

$$\text{SCF}_{\text{Design}} = 1.07 \times \text{SCF}_{\text{Eq. (16)}}. \tag{19}$$

6. Conclusions

Results from 118 validated FE models were used to quantify the influence of key geometric parameters on chord-side SCFs at the crown, toe, and saddle positions of internally ring-stiffened two-planar tubular DKT-joints under axial loading. Based on the analyses, four parametric equations were developed for fatigue design applications. The main conclusions are as follows:

- Increasing τ, β, γ, and θ increases SCFs along the weld toe, whereas increasing η reduces SCFs at all considered locations.
- For arbitrary joint geometries under axial loading, the maximum and minimum SCFs occur at the crown (180°) and outer saddle positions, respectively.
- Internal ring stiffeners significantly reduce SCFs compared to unstiffened DKT-joints, leading to improved fatigue performance. Therefore, existing parametric formulas for unstiffened DKT-joints are not applicable to ring-stiffened configurations, as they substantially overpredict SCFs.
- The proposed parametric equations demonstrate high coefficients of determination and satisfy the acceptance criteria of the UK Department of Energy, confirming their reliability for SCF prediction and fatigue design of axially loaded, internally ring-stiffened two-planar tubular DKT-joints.

References

1. API RP 2A—WSD (2014). Recommended practice for planning, designing and constructing fixed offshore platforms—Working stress design. 22nd Edition, American Petroleum Institute, Washington DC, USA.
2. UK Department of Energy (1983). Background notes to the fatigue guidance of offshore tubular joints. UK DoE, London, UK.

3. Kuang, J.G., Potvin, A.B., Leick, R.D. (1975). Stress concentration in tubular joints. Proceedings of the offshore technology conference, Houston, USA.
4. Efthymiou, M. (1988). Development of SCF formulae and generalized influence functions for use in fatigue analysis. OTJ 88, Surrey, UK.
5. Hellier, A.K., Connolly, M., Dover, W.D. (1990). Stress concentration factors for tubular Y and T-joints. International Journal of Fatigue, 12, 13-23. https://doi.org/10.1016/0142-1123(90)90338-F.
6. UK Health and Safety Executive (1997). OTH 354: Stress concentration factors for simple tubular joints − assessment of existing and development of new parametric formulae. UK HSE, London, UK.
7. Karamanos, S.A., Romeijn, A., Wardenier, J. (2000). Stress concentrations in tubular gap K-joints: mechanics and fatigue design. Engineering Structures, 22, 4-14. https://doi.org/10.1016/S0141-0296(98)00062-5.
8. Gho, W.M., Gao, F. (2004). Parametric equations for stress concentration factors in completely overlapped tubular K(N)-joints. Journal of Constructional Steel Research, 60, 1761-1782. https://doi.org/10.1016/j.jcsr.2004.05.003.
9. Gao F. (2006). Stress and strain concentrations of completely overlapped tubular joints under lap brace OPB load. Thin-Walled Structures, 44, 861-871. https://doi.org/10.1016/j.tws.2006.08.017.
10. Gao, F., Shao, Y.B., Gho, W.M. (2007). Stress and strain concentration factors of completely overlapped tubular joints under lap brace IPB load. Journal of Constructional Steel Research, 63, 305-316. https://doi.org/10.1016/j.jcsr.2006.05.007.
11. Yang, J., Chen, Y., Hu, K. (2015). Stress concentration factors of negative large eccentricity tubular N-joints under axial compressive loading in vertical brace. Thin-Walled Structures, 96, 359-371. https://doi.org/10.1016/j.tws.2015.08.027.
12. Morgan, M.R., Lee, M.M.K. (1998). Parametric equations for distributions of stress concentration factors in tubular K-joints under out-of-plane moment loading. International Journal of Fatigue, 20, 449-461. https://doi.org/10.1016/S0142-1123(98)00011-5.
13. Morgan, M.R., Lee, M.M.K. (1998). Prediction of stress concentrations and degrees of bending in axially loaded tubular K-joints. Journal of Constructional Steel Research, 45(1), 67-97. https://doi.org/10.1016/S0143-974X(97)00059-X.
14. Chang, E., Dover, W.D. (1999). Parametric equations to predict stress distributions along the intersection of tubular X and DT-joints. International Journal of Fatigue, 21, 619-635. https://doi.org/10.1016/S0142-1123(99)00018-3.
15. Chang, E., Dover, W.D. (1999). Prediction of stress distributions along the intersection of tubular Y and T-joints. International Journal of Fatigue, 21, 361-381. https://doi.org/10.1016/S0142-1123(98)00083-8.
16. Shao, Y.B. (2004). Proposed equations of stress concentration factor (SCF) for gap tubular K-joints subjected to bending load. International Journal of Space Structures, 19, 137-147. https://doi.org/10.1260%2F0266351042886667.
17. Shao, Y.B. (2007). Geometrical effect on the stress distribution along weld toe for tubular T- and K-joints under axial loading. Journal of Constructional Steel Research, 63, 1351-1360. https://doi.org/10.1016/j.jcsr.2006.12.005.
18. Shao, Y.B., Du, Z.F., Lie, S.T. (2009). Prediction of hot spot stress distribution for tubular K-joints under basic loadings. Journal of Constructional Steel Research, 65, 2011-2026. https://doi.org/10.1016/j.jcsr.2009.05.004.
19. Lotfollahi-Yaghin, M.A., Ahmadi, H. (2010). Effect of geometrical parameters on SCF distribution along the weld toe of tubular KT-joints under balanced axial loads. International Journal of Fatigue, 32, 703-719. https://doi.org/10.1016/j.ijfatigue.2009.10.008.
20. Ahmadi, H., Lotfollahi-Yaghin, M.A., Aminfar, M.H. (2011). Geometrical effect on SCF distribution in uni-planar tubular DKT-joints under axial loads. Journal of Constructional Steel Research, 67(8), 1282-1291. https://doi.org/10.1016/j.jcsr.2011.03.011.
21. Lotfollahi-Yaghin, M.A., Ahmadi, H. (2011). Geometric stress distribution along the weld toe of the outer brace in two-planar tubular DKT-joints: parametric study and deriving the SCF design equations. Marine Structures, 24, 239-260. https://doi.org/10.1016/j.marstruc.2011.02.005.

22. Liu, G., Zhao, X., Huang, Y. (2015). Prediction of stress distribution along the intersection of tubular T-joints by a novel structural stress approach. International Journal of Fatigue, 80, 216-230. https://doi.org/10.1016/j.ijfatigue.2015.05.021.
23. Karamanos, S.A., Romeijn, A., Wardenier, J. (1999). Stress concentrations in multi-planar welded CHS XX-connections. Journal of Constructional Steel Research, 50, 259-282. https://doi.org/10.1016/S0143-974X(98)00244-2.
24. Chiew, S.P., Soh, C.K., Wu, N.W. (2000). General SCF design equations for steel multiplanar tubular XX-joints. International Journal of Fatigue, 22, 283-293. https://doi.org/10.1016/S0142-1123(99)00130-9.
25. Wingerde, A.M., Packer, J.A., Wardenier, J. (2001). Simplified SCF formulae and graphs for CHS and RHS K- and KK-connections. Journal of Constructional Steel Research, 57, 221-252. https://doi.org/10.1016/S0143-974X(00)00015-8.
26. Karamanos, S.A., Romeijn, A., Wardenier, J. (2002). SCF equations in multi-planar welded tubular DT-joints including bending effects. Marine Structures, 15, 157-173. https://doi.org/10.1016/S0951-8339(01)00020-X.
27. Chiew, S.P., Soh, C.K., Wu, N.W. (1999). Experimental and numerical stress analyses of tubular XT-joint. Journal of Structural Engineering, 125, 1239-1248. https://doi.org/10.1061/(ASCE)0733-9445(1999)125:11(1239).
28. Ahmadi, H., Lotfollahi-Yaghin, M.A., Aminfar, M.H. (2011). Distribution of weld toe stress concentration factors on the central brace in two-planar CHS DKT-connections of steel offshore structures. Thin-Walled Structures, 49, 1225-1236. https://doi.org/10.1016/j.tws.2011.06.001.
29. Ahmadi, H., Lotfollahi-Yaghin, M.A., Aminfar, M.H. (2011). Effect of stress concentration factors on the structural integrity assessment of multi-planar offshore tubular DKT-joints based on the fracture mechanics fatigue reliability approach. Ocean Engineering, 38, 1883-1893. https://doi.org/10.1016/j.oceaneng.2011.08.004.
30. Ahmadi, H., Lotfollahi-Yaghin, M.A. (2012). Geometrically parametric study of central brace SCFs in offshore three-planar tubular KT-joints. Journal of Constructional Steel Research, 71, 149-161. https://doi.org/10.1016/j.jcsr.2011.10.024.
31. Ahmadi, H., Zavvar, E. (2016). The effect of multi-planarity on the SCFs in offshore tubular KT-joints subjected to in-plane and out-of-plane bending loads. Thin-Walled Structures, 106, 148-165. https://doi.org/10.1016/j.tws.2016.04.020.
32. Ahmadi, H., Kouhi, A. (2020). Stress concentration factors of multi-planar tubular XT-joints subjected to out-of-plane bending moments. Applied Ocean Research, 96, 102058. https://doi.org/10.1016/j.apor.2020.102058.
33. Zavvar, E., Rosa-Santos, P., Taveira-Pinto, F. (2025). Analysis of SCF parameters in two planar joints in offshore wind turbine support structures. Journal of Constructional Steel Research, 231, 109608. https://doi.org/10.1016/j.jcsr.2025.109608.
34. Nwosu, D.I., Swamidas, A.S.J., Munaswamy, K. (1995). Numerical stress analysis of internal ring-stiffened tubular T-joints. Journal of Offshore Mechanics and Arctic Engineering, 117, 113-125. https://doi.org/10.1115/1.2827061.
35. Hoon, K.H., Wong, L.K., Soh, A.K. (2001). Experimental investigation of a doubler-plate reinforced tubular T-joint subjected to combined loadings. Journal of Constructional Steel Research, 57, 1015-1039. https://doi.org/10.1016/S0143-974X(01)00023-2.
36. Myers, P.T., Brennan, F.P., Dover, W.D. (2001). The effect of rack/rib plate on the stress concentration factors in jack-up chords. Marine Structures, 14, 485-505. https://doi.org/10.1016/S0951-8339(00)00051-4.
37. Ahmadi, H., Lotfollahi-Yaghin, M.A. (2015). Stress concentration due to in-plane bending (IPB) loads in ring-stiffened tubular KT-joints of offshore structures: Parametric study and design formulation. Applied Ocean Research, 51, 54-66. https://doi.org/10.1016/j.apor.2015.02.009.

38. Ahmadi, H., Zavvar, E. (2015). Stress concentration factors induced by out-of-plane bending loads in ring-stiffened tubular KT-joints of jacket structures. Thin-Walled Structures, 91, 82-95. https://doi.org/10.1016/j.tws.2015.02.011.
39. Xu, F., Chen, J., Jin, W. (2015). Experimental investigation of SCF distribution for thin-walled concrete-filled CHS joints under axial tension loading. Thin-Walled Structures, 93, 149-157. https://doi.org/10.1016/j.tws.2015.03.019.
40. Ahmadi, H., Lotfollahi-Yaghin, M.A., Shao, Y.B., Aminfar, M.H. (2012). Parametric study and formulation of outer-brace geometric stress concentration factors in internally ring-stiffened tubular KT-joints of offshore structures. Applied Ocean Research, 38, 74-91. https://doi.org/10.1016/j.apor.2012.07.004.
41. Ahmadi, H., Lotfollahi-Yaghin, M.A., Shao, Y.B. (2013). Chord-side SCF distribution of central brace in internally ring-stiffened tubular KT-joints: A geometrically parametric study. Thin-Walled Structures, 70, 93-105. https://doi.org/10.1016/j.tws.2013.04.011.
42. Nassiraei, H., Rezadoost, P. (2020). Stress concentration factors in tubular T/Y-joints strengthened with FRP subjected to compressive load in offshore structures. International Journal of Fatigue, 140, 105719. https://doi.org/10.1016/j.ijfatigue.2020.105719.
43. Nassiraei, H., Rezadoost P. (2021). SCFs in tubular X-joints retrofitted with FRP under out-of-plane bending moment. Marine Structures, 79, 103010. https://doi.org/10.1016/j.marstruc.2021.103010.
44. Nassiraei, H., Rezadoost, P. (2021). SCFs in FRP-Strengthened steel tubular X-joints under compression: Parametric Study and Formulation. Proceedings of the 12th international congress on civil engineering, Mashhad, Iran.
45. Nassiraei, H., Rezadoost, P. (2021). SCFs in tubular X-connections retrofitted with FRP under in-plane bending load. Composite Structures, 274, 114314. https://doi.org/10.1016/j.compstruct.2021.114314.
46. Nassiraei, H., Rezadoost, P. (2022). Stress concentration factors in tubular T-joints reinforced with external ring under in-plane bending moment. Ocean Engineering, 266, 12551. https://doi.org/10.1016/j.oceaneng.2022.112551.
47. Nassiraei, H., Rezadoost, P. (2023). Stress concentration factors in tubular T-joints stiffened with external ring under axial load. Ocean Systems Engineering, 13, 43-55. https://doi.org/10.12989/ose.2023.13.1.043.
48. Zavvar, E., Guedes Soares, C. (2022). "Effects of fibre reinforced polymer on stress concentration factors in uniplanar DKT-joints subjected to the compression loading. Trends in maritime technology and engineering, (Eds., Guedes Soares, C. and Santos, T.A.), Taylor and Francis, London, UK.
49. Woghiren, C.O., Brennan, F.P. (2009). Weld toe stress concentrations in multi planar stiffened tubular KK Joints. International Journal of Fatigue, 31, 164-172. https://doi.org/10.1016/j.ijfatigue.2008.03.039.
50. Ahmadi, H., Alinezhad, R., Alizadeh Atalo, A. (2022). Stress concentration analysis of internally ring-stiffened two-planar tubular KK-joints. Ships and Offshore Structures, 17, 2203-2217. https://doi.org/10.1080/17445302.2021.1979922.
51. Ahmadi, H., Lotfollahi-Yaghin, M.A., Aminfar, M.H. (2011). Effect of stress concentration factors on the structural integrity assessment of multi-planar offshore tubular DKT-joints based on the fracture mechanics fatigue reliability approach. Ocean Engineering, 38, 1883-1893. https://doi.org/10.1016/j.oceaneng.2011.08.004.
52. Gaspar, B., Garbatov, Y., Guedes Soares, C. (2011). Effect of weld shape imperfections on the structural hot-spot stress distribution. Ships and Offshore Structures, 6(1-2), 145-159. https://doi.org/10.1080/17445302.2010.497052.
53. Ahmadi, H., Lotfollahi-Yaghin, M.A. (2012). A probability distribution model for stress concentration factors in multi-planar tubular DKT-joints of steel offshore structures. Applied Ocean Research, 34, 21-32. https://doi.org/10.1016/j.apor.2011.11.002.
54. Ahmadi, H., Lotfollahi-Yaghin, M.A. (2013). Effect of SCFs on S–N based fatigue reliability of multi-planar tubular DKT-joints of offshore jacket-type structures. Ships and Offshore Structures, 8, 55-72. https://doi.org/10.1080/17445302.2011.627750.

55. Ahmadi, H., Mohammadi, A.H., Yeganeh, A. (2015). Probability density functions of SCFs in internally ring-stiffened tubular KT-joints of offshore structures subjected to axial load. Thin-Walled Structures, 94, 485-499. https://doi.org/10.1016/j.tws.2015.05.012.
56. Ahmadi, H., Mohammadi, A.H., Yeganeh, A., Zavvar, E. (2016). Probabilistic analysis of stress concentration factors in tubular KT-joints reinforced with internal ring stiffeners under in-plane bending loads. Thin-Walled Structures, 99, 58-75. https://doi.org/10.1016/j.tws.2015.11.010.
57. Ahmadi, H. (2016). A probability distribution model for SCFs in internally ring-stiffened tubular KT-joints of offshore structures subjected to out-of-plane bending loads. Ocean Engineering, 116, 184-199. https://doi.org/10.1016/j.oceaneng.2016.02.037.
58. Ahmadi, H., Mousavi Nejad Benam, M.A. (2017). Probabilistic analysis of SCFs in unstiffened gap tubular KT-joints of jacket structures under the OPB moment loads. Advances in Structural Engineering, 20, 595-615. https://doi.org/10.1177%2F1369433216658487.
59. Nassiraei, H., Rezadoost, P. (2022). Development of a probability distribution model for the SCFs in tubular X-connections retrofitted with FRP. Structures, 36, 233-247. https://doi.org/10.1016/j.istruc.2021.10.033.
60. Nassiraei, H., Rezadoost, P. (2022). Probabilistic analysis of the SCFs in tubular T/Y-joints reinforced with FRP under axial, in-plane bending, and out-of-plane bending loads. Structures, 35, 1078-1097. https://doi.org/10.1016/j.istruc.2021.06.029.
61. Azari Dodaran, N., Ahmadi, H., Lotfollahi-Yaghin, M.A. (2018). Parametric study on structural behavior of tubular K-joints under axial loading at fire-induced elevated temperatures. Thin-Walled Structures, 130, 467-486. https://doi.org/10.1016/j.tws.2018.06.014.
62. Azari-Dodaran, N., Ahmadi, H., Lotfollahi-Yaghin, M.A. (2018). Static strength of axially loaded tubular KT-joints at elevated temperatures: Study of geometrical effects and parametric formulation. Marine Structures, 61, 282-308. https://doi.org/10.1016/j.marstruc.2018.06.009.
63. Azari-Dodaran, N., Ahmadi, H. (2019). Static behavior of two-planar tubular KT-joints under axial loading at fire-induced elevated temperatures. Ocean Engineering and Science, 4, 352-372. https://doi.org/10.1016/j.joes.2019.05.009.
64. Nassiraei, H. (2019). Static strength of tubular T/Y-joints reinforced with collar plates at fire induced elevated temperature. Marine Structures, 67, 102635. https://doi.org/10.1016/j.marstruc.2019.102635.
65. Nassiraei, H. (2023). Probability distribution models for the ultimate strength of tubular T/Y-joints reinforced with collar plates at room and different fire conditions. Ocean Engineering, 270, 113557. https://doi.org/10.1016/j.oceaneng.2022.113557.
66. Nassiraei, H. (2024). Probabilistic analysis of strength in retrofitted X-joints under tensile loading and fire conditions. Buildings, 14, 2105. https://doi.org/10.3390/buildings14072105.
67. Nassiraei, H. (2024). Probability distribution functions for the ultimate strength of X-joints with collar plates in compressive load at room and fire conditions. Structures, 59, 105703. https://doi.org/10.1016/j.istruc.2023.105703.
68. Nassiraei, H. (2025). Optimal probability function for ultimate resistance of offshore T/Y-connections enhanced with collar plates under compression, tension, and bending loads. Scientific Reports, 15, 36807. https://doi.org/10.1038/s41598-025-20725-z.
69. Zavvar, E., Rosa-Santos, P., Ghafoori, E., Taveira-Pinto, F. (2025). Analysis of tubular joints in marine structures: A comprehensive review. Marine Structures, 99, 103702. https://doi.org/10.1016/j.marstruc.2024.103702.
70. Ahmadi, H., Asoodeh, S. (2016). Parametric study of geometrical effects on the degree of bending (DoB) in offshore tubular K-joints under out-of-plane bending loads. Applied Ocean Research, 58, 1-10. https://doi.org/10.1016/j.apor.2016.03.004.
71. Nassiraei, H., Asgarian, B., Rezadoost, P. (2025). Degree of bending in X-connections retrofitted with different types of fiber-reinforced polymers subjected to axial load. Structures, 71, 107964. https://doi.org/10.1016/j.istruc.2024.107964.
72. Nassiraei, H. (2025). Probabilistic modeling of degree of bending in FRP-strengthened offshore tubular X-joints. Scientific Reports, 15, 39284. https://doi.org/10.1038/s41598-025-23024-9.

73. Ahmadi, H., Ziaei Nejad, A. (2017). Local joint flexibility of two-planar tubular DK-joints in OWTs subjected to axial loading: Parametric study of geometrical effects and design formulation. Ocean Engineering, 136, 1-10. https://doi.org/10.1016/j.oceaneng.2017.03.011.
74. Nassiraei, H. (2019). Local joint flexibility of CHS X-joints reinforced with collar plates in jacket structures subjected to axial load. Applied Ocean Research, 93, 101961. https://doi.org/10.1016/j.apor.2019.101961.
75. Nassiraei, H. (2020). Local joint flexibility of CHS T/Y-connections strengthened with collar plate under in-plane bending load: Parametric study of geometrical effects and design formulation. Ocean Engineering, 202, 107054. https://doi.org/10.1016/j.oceaneng.2020.107054.
76. Nassiraei, H. (2022). Geometrical effects on the LJF of tubular T/Y-joints with doubler plate in offshore wind turbines. Ships and Offshore Structures, 17, 481-491. https://doi.org/10.1080/17445302.2020.1835051.
77. Nassiraei, H. (2025). Identification of the most suitable probability models for local joint flexibility in T/Y-connections stiffened with collar or doubler plates. Results in Engineering, 25, 104387. https://doi.org/10.1016/j.rineng.2025.104387.
78. Ahmadi, H., Akhtegan, M. (2022). Effects of geometrical parameters on the local joint flexibility (LJF) of three-planar tubular T-joints in offshore structures. Ships and Offshore Structures, 17, 1604-1615. https://doi.org/10.1080/17445302.2021.1937794.
79. Ahmadi, H., Akbari Niri, A. (2024). Geometrical effects on the local joint flexibility of three-planar tubular Y-joints in substructures of offshore wind turbines. Ships and Offshore Structures, 19, 484-496. https://doi.org/10.1080/17445302.2023.2179213.
80. Lee, M.K., Wilmshurst, S.R. (1995). Numerical modeling of CHS joints with multiplanar double-K configuration. Journal of Constructional Steel Research, 32, 281-301. https://doi.org/10.1016/0143-974X(95)93899-F.
81. Cao, J.J., Yang, G.J., Packer, J.A. (1997). FE mesh generation for circular tubular joints with or without cracks. Proceedings of the 7th international offshore and polar engineering conference, Honolulu, USA.
82. Lee, M.M.K. (1999). Strength, stress and fracture analyses of offshore tubular joints using finite elements. Journal of Constructional Steel Research, 51, 265-286. https://doi.org/10.1016/S0143-974X(99)00025-5.
83. Shao, Y.B. (2004). Fatigue behaviour of uni-planar CHS gap K-joints under axial and in-plane bending loads. Ph.D. Dissertation, Nanyang Technological University, Singapore.
84. AWS D 1.1 (2002). Structural welding code. American Welding Society, Miami, USA.
85. Ahmadi, H., Lotfollahi-Yaghin, M.A., Aminfar, M.H. (2012). The development of fatigue design formulas for the outer brace SCFs in offshore three-planar tubular KT-joints. Thin-Walled Structures, 58, 67-78. https://doi.org/10.1016/j.tws.2012.04.011.
86. Smedley, P., Fisher, P. (1991). Stress concentration factors for simple tubular joints. Proceedings of the international offshore and polar engineering conference (ISOPE), Edinburgh, Scotland.
87. N'Diaye, A., Hariri, S., Pluvinage, G., Azari, Z. (2007). Stress concentration factor analysis for notched welded tubular T-joints. International Journal of Fatigue, 29, 1554-1570. https://doi.org/10.1016/j.ijfatigue.2006.10.030.
88. IIW-XV-E (1999). Recommended fatigue design procedure for welded hollow section joints, IIW Docs, XV-1035-99/XIII-1804-99. International Institute of Welding, France.
89. Ahmadi, H. (2012). Experimental and numerical investigation of the SCF distribution in unstiffened and stiffened uniplanar tubular KT-joints of steel platforms and the extension of numerical study to multi-planar joints. PhD Dissertation, University of Tabriz, Iran (In Farsi).
90. Chang, E., Dover, W.D. (1996). Stress concentration factor parametric equations for tubular X and DT joints. International Journal of Fatigue, 18(6), 363-387. https://doi.org/10.1016/0142-1123(96)00017-5.
91. Underwater Engineering Group (1985). Design of tubular joints for offshore structures. UEG/CIRIA, London, UK.
92. Efthymiou, M., Durkin, S. (1985). Stress concentrations in T/Y and gap/overlap K-joints. Proceedings of the conference on behavior of offshore structures, Delft, Netherlands.

93. Bomel Consulting Engineers (1994). Assessment of SCF equations using Shell/KSEPL finite element data. C5970R02.01 REV C, Bomel Consulting Engineers.

Nomenclature

DoB	Degree of bending
DoE	Department of Energy
FE	Finite elements
HSS	Hot-spot stress
IPB	In-plane bending
LJF	Local joint flexibility
OPB	Out-of-plane bending
SCF	Stress concentration factor
d	Outer diameter of the brace
D	Outer diameter of the chord
F_a	Axial force of brace
g	Gap
L	Chord length
R^2	Coefficient of determination
t	Brace wall thickness
T	Chord wall thickness
w_s	Ring width
$X_\perp$	Direction perpendicular to the weld toe
α	Chord slenderness ratio ($= 2L/D$)
α_B	Brace slenderness ratio ($= 2l/d$)
β	Brace-to-chord diameter ratio ($= d/D$)
η	Ring width to chord diameter ratio ($= w_s/D$)
γ	Chord wall slenderness ratio ($= D/2T$)
ψ	Dihedral angle
$\sigma_{\perp W}$	Extrapolated geometric stress at weld toe
$\sigma_{\perp E}$	Stress at extrapolation point normal to weld toe
σ_n	Nominal stress
τ	Brace-to-chord thickness ratio ($= t/T$)
θ	Brace inclination angle
ζ	Relative gap ($= g/D$)